Int. J. Therm. Sci. (2000) 39, 414–421

S1290-0729(00)00214-3/FLA

Velocity distribution and vibration excitation in tube bundle heat exchangers

Ulrich Mohr *, Horst Gelbe

Technical University Berlin, Institute of Process and Plant Technology, Straße des 17. Juni 135, Sekr. KF1, D-10623 Berlin, Germany

(Received 3 May 1999, accepted 7 September 1999)

Abstract — Design criteria for tube bundle heat exchangers, to avoid fluidelastic instability, are based on stability criteria for ideal bundles and uniform flow conditions along the tube length. In real heat exchangers, a non-uniform flow distribution is caused by inlet nozzles, impingement plates, baffles and bypass gaps. The calculation of the equivalent velocities, according to the extended stability equation of Connors, requires the knowledge of the mode shape and the assumption of a realistic velocity distribution in each flow section of the heat exchanger. It is the object of this investigation to derive simple correlations and recommendations, (1) for equivalent velocity distributions, based on partial constant velocities, and (2) for the calculation of the critical volume flow in practical design applications. With computational fluid dynamic (CFD) programs it is possible to calculate the velocity distribution in real tube bundles, and to determine the most endangered tube and thereby the critical volume flow. The paper moreover presents results and design equations for the inlet section of heat exchangers with variations of a broad range of geometrical parameters, e.g., tube pitch, shell diameter, nozzle diameter, span width, distance between nozzle exit and tube bundle. © 2000 Éditions scientifiques et médicales Elsevier SAS

vibration excitation / tubes and tube bundles / CFD simulation / velocity distribution in tube bundle heat exchangers

Nomenclature

a	distance between shell periphery and the first tube row (see *figure 1*)	mm
b	distance between nozzle exit and the first tube row (see *figure 1*)	mm
b^*	$= b/d_a$	
c_n	correction factor considering the influence of the number of tube row exposed to the approaching flow on the excitation force	
d_a	tube outer diameter	mm
D_M	shell inside diameter	mm
d_S	nozzle diameter	mm
f	natural frequency	Hz
F_q	cross-sectional area	mm^2
K	stability constant (see equation (1))	
K^*	stability ratio (see equation (4))	
L	tube length or partial length of a tube with constant velocity	mm
m	total tube mass per unit length	$kg{\cdot}m^{-1}$
N	number of flow sections or partial flow sections	
P	exponent of mass-damping factor (see equation (1))	
R	number of partial flow sections between two baffles	
s	chord length/width of the cross-sectional area	mm
S	energy ratio (see equation (3))	
u	gap velocity (see equation (3))	$m{\cdot}s^{-1}$
u^*	dimensionless gap velocity (see equation (1))	
$\dot{V}$	volume flow rate	$m^3{\cdot}s^{-1}$
v_S	velocity in the nozzle	$m{\cdot}s^{-1}$
X	jet expansion factor (see equation (13))	
z	coordinate along the tube length	mm
Δ	mass-damping parameter $= m\Lambda(\rho \cdot d_a^2)^{-1}$	
ΔS	partial energy ratio (see equation (6))	
Λ	logarithmic decrement of damping	
ρ	density of the shell fluid	$kg{\cdot}m^{-3}$
τ	tube pitch ratio (see equation (3))	
Φ	mode shape function (see equation (3))	
Ψ	velocity distribution function	

Indices

n	number of tube row approached by flow

* Correspondence and reprints.
mohr@tk1.fb10.tu-berlin.de

r	flow section or partial flow section number
cr.	critical value
$\sim$	equivalent value
$\hat{}$, max	maximum value

1. INTRODUCTION

For a safe design of real heat exchangers, to avoid damages caused by fluid-elastic instability, the effective velocity distribution over the entire tube length should be known, particularly in the section with nozzle inlet and in the baffle windows. Up to now only rough assumptions, as shown later on in *figure 4* as methods A and B, are possible [1]. Computational fluid dynamic (CFD) programs enable the calculation of the flow field in tube bundle heat exchangers [2]. By parameter studies the influence of the geometry can be investigated. Correlating the calculated velocities with the mode shape function, and regarding the design criteria accepted for ideal bundles, the vibration excitation can be simulated for each tube in the complex geometry, described by the stability ratio K^*, as defined in equation (4). The maximum value of K^* determines the critical volume flow $\dot{V}_{\mathrm{cr.}}$.

By variation of the inlet geometry, it becomes possible to derive simple correlations for equivalent velocity distributions and corresponding flow areas in tube bundle heat exchangers. The three-dimensional steady-state flow field on the shell side of heat exchangers with rigid tubes is calculated using the commercial CFD program STAR-CD. The program solves the well know 3D Navier–Stokes equations for incompressible turbulent flow by using the standard $k-\varepsilon$ model.

2. THEORETICAL BACKGROUND

The correlation between the mode shape and the velocity distribution suggested by Connors [3] was already experimentally confirmed by Jahr and Gelbe [4] and by Jahr [5]. Applying the extended stability equation,

$$u^*_{\mathrm{cr.}} = \frac{\tilde{u}_{\mathrm{cr.}}}{f d_{\mathrm{a}}} = K \Delta^P \tag{1}$$

and the equivalent critical velocity,

$$\tilde{u}_{\mathrm{cr.}} = \hat{u}_{\mathrm{cr.}} \sqrt{S} \tag{2}$$

it is possible to convert the stability criteria for ideal bundles and uniform flow conditions to real conditions, using the energy ratio S and the maximum gap velocity $\hat{u}_{\mathrm{cr.}}$. The equivalent velocity $\tilde{u}$ is the velocity, which causes the same vibration excitation at ideal flow conditions. The corresponding critical values $\tilde{u}_{\mathrm{cr.}}$ were taken from Gelbe et al. [6] or Schröder et al. [7]. The energy ratio S is defined by

$$S = \frac{\int_0^L \Psi^2(z) \Phi^2(z)\,\mathrm{d}z}{\int_0^L \Phi^2(z)\,\mathrm{d}z} \quad \text{with } \Psi(z) = \frac{u(z)}{\hat{u}} \tag{3}$$

In order to define the vibration excitation of one tube in inhomogeneous flow, it is necessary to consider the velocity distributions in the tube gaps of that tube and to correlate this velocities with the mode shape function $\Phi(z)$. The mode shape function has been determined in subroutines with finite element methods (FEM) or for simple cases with analytical equations. The stability ratio K^* defines the graduation of the vibration excitation of one tube,

$$K^* = \frac{\tilde{u}}{c_n u_{\mathrm{cr.}}} \tag{4}$$

c_n is a correction factor ≥ 1, considering the influence of the tube rows on the excitation force; c_n is one for the most endangered tube rows (e.g., $n = 2$ for 30° and $n = 3$ for 60° tube arrangements), $c_n > 1$ for the other tube rows, depending on tube array and the pitch ratio. If $\tilde{u} = c_n \tilde{u}_{\mathrm{cr}}$, $K^* = 1$, e.g., the tube becomes critical. When the gap velocities in the partial flow sections r are constant, then the equivalent velocity $\tilde{u}$ can be calculated by equations (5) and (6):

$$\tilde{u} = \hat{u} \sqrt{\sum_{r=1}^{N} \Psi_r^2 \Delta S_r} \tag{5}$$

with the partial energy ratio

$$\Delta S_r = \frac{\int_{L_r} \Phi^2(z)\,\mathrm{d}z}{\int_0^L \Phi^2(z)\,\mathrm{d}z} \tag{6}$$

If the stability ratio for the most endangered tube in the bundle $K^*_{\mathrm{max}} = 1$, the critical volume flow rate can be calculated:

$$\dot{V}_{\mathrm{cr.}} = \hat{u}_{\mathrm{cr.}} \sum_{r=1}^{R} \Psi_r F_{\mathrm{q}r} \tag{7}$$

$F_{\mathrm{q}r}$ is the cross-sectional area for the partial flow section r. Equation (7) is valid for each flow section between two baffles.

TABLE I
Variation of the geometrical parameters.

tube arrangement	30°
outer tube diameter	25 mm
tube pitch ratio τ	1.28; 1.4; 2.0
shell diameter D_M	400, 600, 700, 1200 mm
inlet nozzle diameter d_S	100, 150, 200, 250, 300, 350 mm
support length L	600 mm, 1000 mm
reduced distance between nozzle exit and the first tube row, $b^* = b/d_a$	−0.4 up to 9.0

3. INVESTIGATION OF THE INLET SECTION GEOMETRY

The flow distribution in different inlet sections of tube bundle heat exchangers has been investigated. The tubes first are supported in two fixed bearings, so the support length is equal to the tube length L. The investigation of a one-pass section is justified, since the velocity distribution in the inlet section is independent of the flow in the following sections of a multi-span heat exchanger; designing real heat exchangers, only the relative velocity values $u/\hat{u}$ have to be considered. The nozzles are placed in the middle of the tube length, so, in this first investigation, the velocity distributions and the mode shape functions are symmetrical. *Table I* shows the investigated geometrical parameters.

In *figure 1* the tube layout of one of the investigated bundles is outlined. The distances a or b are varied by removing tube rows, beginning at the nozzle.

Calculating the steady-state flow field, a constant volume flow rate $\dot{V}$ was fixed, in order to determine the axial velocity distribution in the tube gaps. The velocities in the six gaps of each tube with the neighbouring tubes are analysed. The fluid at the shell-side is air at normal conditions. By applying the extended Connors equation, the equivalent velocities for each gap are achieved. The root mean square values of the equivalent velocities of the opposite gaps are determined. With these three average equivalent velocities it is possible to define the approach flow direction and two stability ratios: the first $K^*(30°)$ value is defined for the normal approach flow direction, using the maximum of the three equivalent velocities and the critical velocity for the 30° tube array, the second $K^*(60°)$ value is determined with the two average equivalent velocities in transversal flow direction and a critical value $u_{cr.}$, which is estimated as a linear relation of the critical velocities $u_{cr.}(30°)$ and $u_{cr.}(60°)$, depending on the angle of the flow direction. The basis of this procedure was confirmed by analysing the experimental

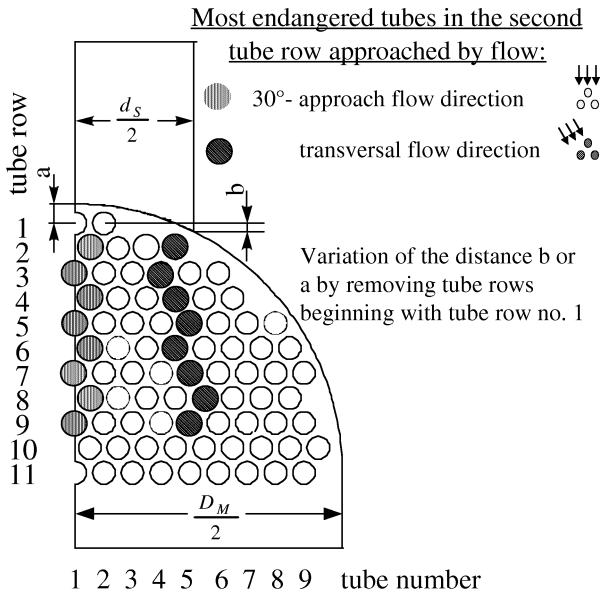

Figure 1. Sketch of a tube bundle with the endangered tubes in the second tube row approached by flow ($D_M = 600$ mm, $L = 1000$ mm, $d_S = 250$ mm, $\tau = 1.28$).

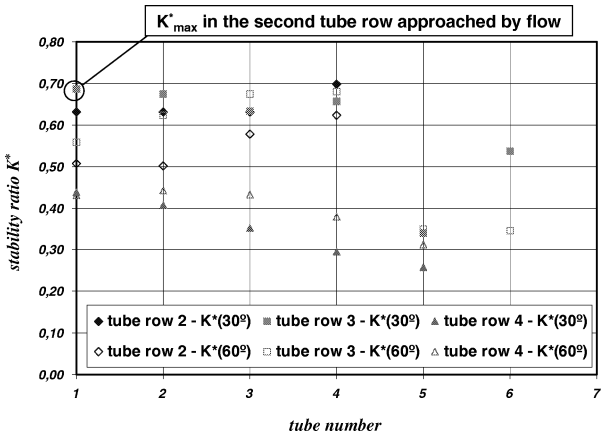

Figure 2. Stability ratio for the tubes in the first three rows approached by flow in a bundle with a reduced distance $b^* = 0.73$ and a volume flow rate $\dot{V} = 1.93$ m^3·s^{-1} ($D_M = 600$ mm, $L = 1000$ mm, $d_S = 250$ mm, $\tau = 1.28$, tube row 1 removed).

measurements of Yeung and Weaver [8]. The c_n values for 30° and 60° tube arrays were taken from the measurements of Andjelic [9], Austermann [10] and Jahr [5]. The results concerning the influence of the transversal flow direction in 30° tube arrangements will be published separately [11].

In *figure 1* the endangered tubes for both K^* values in the second tube row approached by flow are shown. *Figure 2* shows as an example the K^* values for all

TABLE II
Correction factors c_n for the first, second and third tube row exposed to flow in a 30° tube array with $\tau = 1.28$.

n	c_n for $K^*(30°)$	c_n for $K^*(60°)$
1	1.5	1.6
2	1.0	1.0
3	1.1	1.0

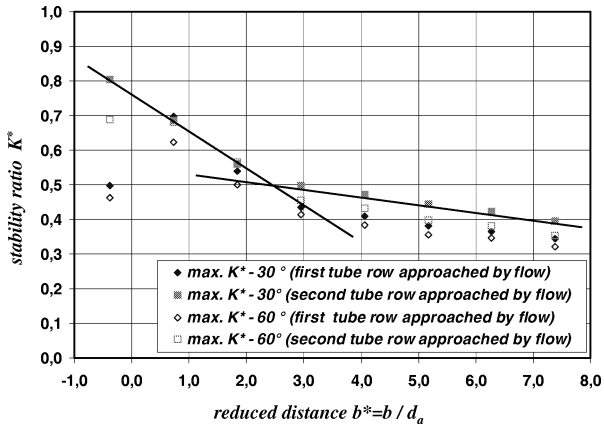

Figure 3. Stability ratio K^* dependent on the reduced distance between the first tube row and the nozzle exit ($D_M = 600$ mm, $L = 1000$ mm, $d_S = 250$ mm, $\tau = 1.28$).

tubes in the first three tube rows approached by flow at a reduced distance $b^* = 0.73$, that means, without the tube row No. 1. The volume flow rate was $\dot{V} = 1.93\ \mathrm{m^3 \cdot s^{-1}}$.The correction factors c_n used in this case are listed in *table II*.

Experimental data by Jahr [5] show that in homogeneous flow and in ideal bundles, the second row becomes first critical, the first row only at about 50 % higher throughput, depending on τ. The reason is the lower upstream velocity of the first row and thereby a lower force on the tube, even though the gap velocities are the same in the first and the second tube row. The highest K^* values were taken in the second row. This value determines the value of the critical volume flow rate,

$$\dot{V}_{\mathrm{cr.}} = \frac{\dot{V}}{K^*_{\mathrm{max}}} \tag{8}$$

The maximum values of the stability ratios K^* of the tubes in the first and the second actual tube row are plotted in *figure 3* as a function of the reduced distance b^* for the described bundles. The highest value of $K^* = 0.8$ appears for normal triangular flow direction ($K^*(30°)$) on the tube number 1 of tube row No. 2, when the shell is

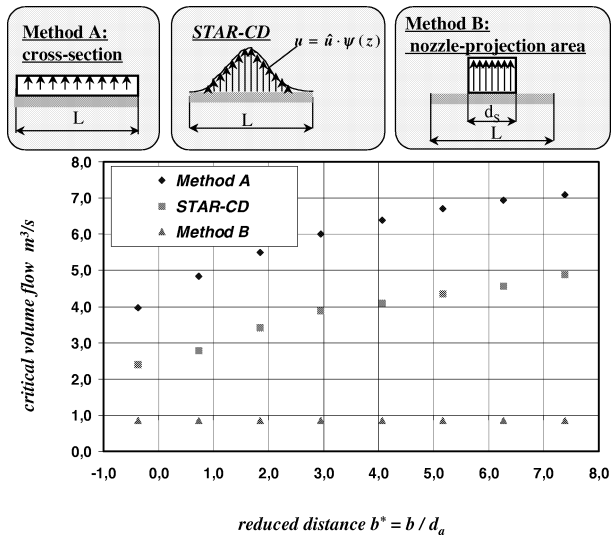

Figure 4. Comparison of the critical volume flow rate in a single-span heat exchanger with simple design methods ($D_M = 600$ mm, $L = 1000$ mm, $d_S = 250$ mm, $\tau = 1.28$).

completely filled out with tubes. This tube layout should be avoided. The highest K^* values are achieved for the normal triangular flow direction in the second tube row approached by flow. Only at $b^* = 0.73$, the calculated K^* value in the first actual tube row is a little bit higher than the maximum value in the second actual tube row, and the $K^*(60°)$ values get up to the value of K^*_{max} (as can be seen from *figure 2*, tube No. 4); that is due to the peak transversal velocity at the nozzle exit. Moreover, in *figure 3* it is shown that the transversal flow direction is not critical. This is true for all investigated bundles with a pitch ratio of $\tau = 1.28$. Two nearly linear functions for the stability ratio between $0 \le b^* \le 2.5$ and for $b^* > 2.5$ can be determined. The value of about $b^* = 2.5$ seems to be a good choice, but b^* should not be lower than 1.

The results for the $K^*(60°)$ values of the other investigated pitch ratios will be presented in [11]. In the further sections of the paper all results are presented for the calculated stability ratios of the normal triangular flow direction $K^*(30°)$.

In *figure 4* the critical volume flow rates, calculated by the described method with STAR-CD, are plotted over the reduced distance b^*. These results are compared with two different simple design methods. In method A a uniform flow in the cross-sectional area is supposed. That is not admissible in this case, because the predicted critical volume flow rates are too high. In method B it is assumed that the flow toward the bundle and the second row occurs only in the nozzle-projection area. The design by method B achieves values being too low

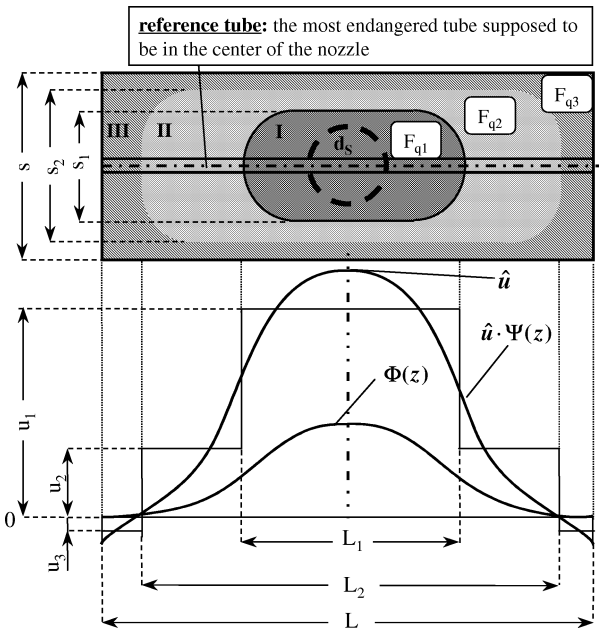

Figure 5. Model for the determination of the velocity distribution and the flow areas.

by a factor of 2–3. Surely, these considerable differences for one-through-flow will become lower in real heat exchangers, depending on the number of flow sections. It is the object of this investigation to find a combination of the two methods A and B, getting a safe prediction of the "measured" (i.e. calculated by STAR-CD) critical volume flow rates.

4. MODEL FOR THE VELOCITY DISTRIBUTION AND THE FLOW AREAS

The model does not describe the true velocity distribution, but the equivalent velocities, i.e. the excitation force on the most endangered tube will be approximated. In *figure 5*, the basic data of the model for determining the distribution of the equivalent velocities and the corresponding flow areas in the second tube row are shown. L is the support length of the tubes and s is length of the chord in the second tube row. The model has been developed and tested for a central position of the inlet nozzle and for a symmetrical mode shape function. It assumes that the most endangered tube is located in the center of the nozzle.

Three flow sections with partial constant velocities have been distinguished in the model:

(I) maximum flow under the inlet nozzle with the cross-sectional area F_{q1} and the equivalent velocity u_1. All other velocities are referred to this highest value, i.e. the velocity ratio $\Psi_1 = 1$,

(II) lower positive flow with the cross-sectional area F_{q2} and the velocity ratio $\Psi_2 = u_2/u_1$,

(III) possible negative recirculation flow with the cross-sectional area F_{q3} and $\Psi_3 = u_3/u_1$.

The flow rate in the partial section III is about 2−10 % of the total flow rate, but the equivalent velocity is negligible, since the mode shape function Φ is nearly zero. The reduction of the flow area by F_{q3} is more important. So, the equivalent velocity u_3 was assumed to be zero.

The first condition is the assumption, that the true velocities $u(z)$ and the model values u_r should produce the same excitation force in each partial section r. For example, the equivalent velocity u_1 in *figure 5* is calculated by taking into account the velocity distribution $u_{cr.}(z)$ and the mode shape function $\Phi(z)$ only in the partial section I along the length L_1:

$$u_1 = \hat{u}_{cr.}\sqrt{\frac{\int_{L_1}\Psi^2(z)\Phi^2(z)\,dz}{\int_{L_1}\Phi^2(z)\,dz}} \tag{9}$$

The equivalent velocities u_2 and u_3 are calculated analogous to equation (9) along the partial length $(L_2 - L_1)$ or $(L - L_2)$.

The second condition is, that the sum of the partial volume flow rates in the partial sections I and II results the critical volume flow rate; the back stream in partial section III is neglected:

$$u_1 F_{q1} + u_2 F_{q2} = \dot{V}_{cr.} \tag{10}$$

The cross-sectional area F_{q1} can be calculated by the length L_1 and the width s_1:

$$F_{q1} = \begin{cases} \left(L_1 s_1 - \left(1-\frac{\pi}{4}\right)s_1^2\right)\left(\frac{\tau-1}{\tau}\right), & s_1 \le L_1 \\ \left(L_1 s_1 - \left(1-\frac{\pi}{4}\right)L_1^2\right)\left(\frac{\tau-1}{\tau}\right), & s_1 \ge L_1 \end{cases} \tag{11}$$

The cross-sectional area F_{q2} is defined by

$$F_{q2} = (L_2 s_2 - L_1 s_1)\left(\frac{\tau-1}{\tau}\right) \tag{12}$$

The bulk flow length L_1 depends on the inlet nozzle diameter d_S, the ratio of support to chord length and a

fitting parameter, the jet expansion factor X:

$$L_1 = d_S X \frac{L}{s} \tag{13}$$

The jet expansion factor is a function of the reduced distance between the first row and the nozzle exit $b^* = b/d_a$; the more tube rows are removed from the bundle, the more the bulk flow can expand.

The width s_1 depends also on Xd_S and in addition on the pitch ratio and the geometrical relations of the nozzle diameter and the support length to the shell diameter. These influences are given by the corrective functions f_1 (equation (18)) and f_2 (equation (19)):

$$s_1 = X d_S f_1\left(\tau, \frac{D_M}{L}, \frac{D_M}{d_S}\right) \tag{14}$$

If the reduced nozzle diameter d_S/L is high, then no recirculation occurs and $L_2 = L$. The length L_2 can be determined by the "measured" (i.e. the calculated values by STAR-CD) flow distribution. In *figure 6* the velocity distribution in the tube gaps, refered to the velocity in the nozzle v_S, for one geometry (shell diameter $D_M = 700$ mm, support length $L = 600$ mm, nozzle diameter $d_S = 300$ mm, pitch ratio $\tau = 2.0$, $b^* = 2.25$) is illustrated. The marked line shows the velocity distribution for the most endangered tube in the tube gap No. 1. At the intersection of this line with the neutral point line, the length L_2 can be found. The profiles of the velocities in the tube gaps Nos. 2 and 3 are very similar; the values are negligibly lower. The tube gap No. 4, placed outside the nozzle-projection area shows significant lower velocity values, which reduce further for the tube gaps Nos. 5 and 6. *Figure 6* contains also the values of the length L_1/L and the equivalent velocities u_1/v_S and u_2/v_S, calculated by the model equations.

The results for the reduced flow length L_2/L of all investigated tube bundles are illustrated in *figure 7*. To avoid recirculation, the nozzle diameters have to exceed values $d_S \geq (0.33 \text{ to } 0.5)L$, depending on the pitch ratio τ. The following functions for the reduced length L_2 could be obtained:

$$\frac{L_2^*}{L} = 1.5 f_2(\tau)\left(\frac{d_S}{L} + 0.2\right)^{0.7}, \tag{15}$$

$$L_2 = L_2^* \leq L \tag{16}$$

The width s_2 of the cross-sectional area F_{q2} is calculated by a similar equation, which considers the same

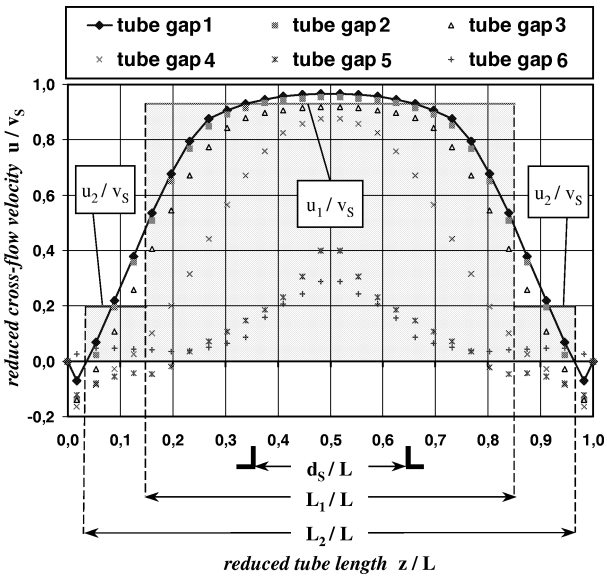

Figure 6. Axial and radial velocity distribution in the tube gaps of the second row approached by flow ($D_M = 700$ mm, $L = 600$ mm, $d_S = 300$ mm, $\tau = 2.0$, $b^* = 2.25$).

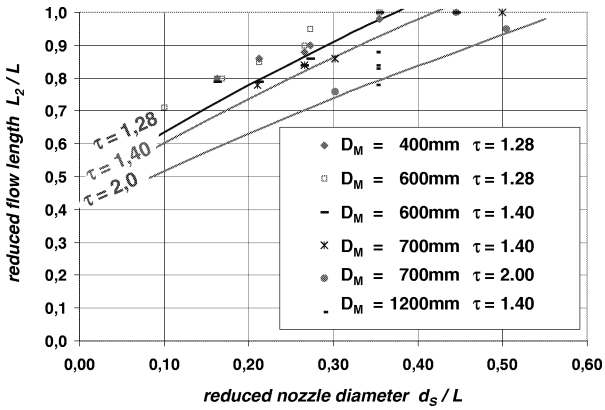

Figure 7. Reduced flow length L_2/L as a function of the reduced nozzle diameter and the pitch ratio.

corrective function as in equation (14):

$$\frac{s_2}{s} = 1.42 f_1\left(\tau, \frac{D_M}{L}, \frac{D_M}{d_S}\right)\left(\frac{d_S}{s} + 0.2\right)^{0.7} \tag{17}$$

The corrective functions f_1 and f_2 are given by the equations (18) and (19):

$$f_1\left(\tau, \frac{D_M}{L}, \frac{D_M}{d_S}\right) = 0.34\frac{\tau}{\tau - 1}\left(\frac{D_M}{L}\right)^{0.3}\left(1 - 0.09\frac{D_M}{d_S}\right) \tag{18}$$

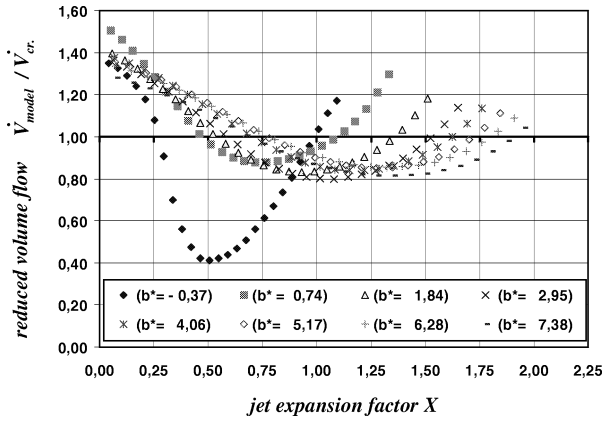

Figure 8. Determination of the jet expansion factor X ($D_M = 600$ mm, $L = 1000$ mm, $d_S = 250$ mm, $\tau = 1.28$).

$$f_2(\tau) = 0.6\frac{\tau}{\tau - 0.5} \tag{19}$$

In order to determine the jet expansion factors X, the reduced volume flows ($\dot{V}_{\text{model}}/\dot{V}_{\text{cr.}}$) are plotted over all variants of X. *Figure 8* shows an example. The searched solutions are found for such values of the jet expansion factor, where the volume flow rate, calculated by the model, is equal to the critical volume flow rate, calculated by STAR-CD. There are two solutions, but the solutions at the lower X values are not always plausible (e.g., $L_1 < d_S$). For this reason the higher X values were taken. In *figure 8* it can be observed that near the minima the influence of the jet expansion factor is not significant, except the noncommendable case $b^* = -0.375$. The curves are clear graduated, so, increasing the reduced distance b^*, the jet expansion factor also increases. The analysis showed that the distance a (see *figure 1*) was not suitable correlating the values of X. The distance b is the appropriate parameter considering the influence of the nozzle diameter and to define, whether the first row overlaps the nozzle flow area, which should be ensured choosing $b^* \geq 1.0$.

In *figure 9* all values of the jet expansion factor X for $D_M = 600$ and 700 mm are plotted over the reduced distance b^*. For a safe design the following function can be defined:

$$X = 1.2(b^*)^{0.2} \geq 1.0 \tag{20}$$

For values $b^* < 0.4$, i.e. those shells, which are completely filled with tubes, there is $X = 1.0$. By this function and by the derived equations, the cross-sectional areas F_{q1} and F_{q2} can be calculated.

In *figure 10* the velocity ratio $\Psi_2 = u_2/u_1$ is plotted over the reduced difference length $(L_2^* - L_1)/L$, L_2^* being calculated by equation (15), also when L_2^* should be

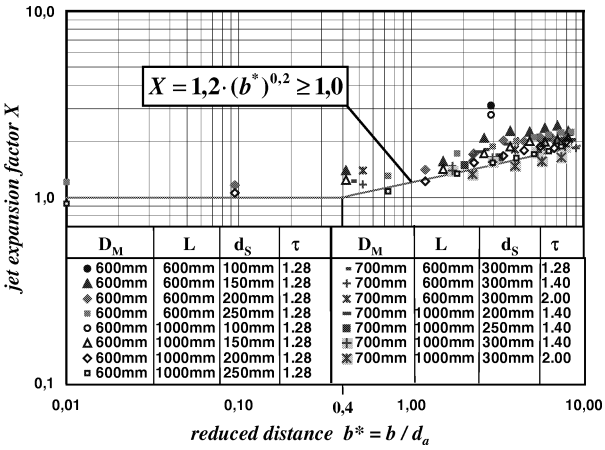

Figure 9. Jet expansion factor X depending on the reduced distance b^*.

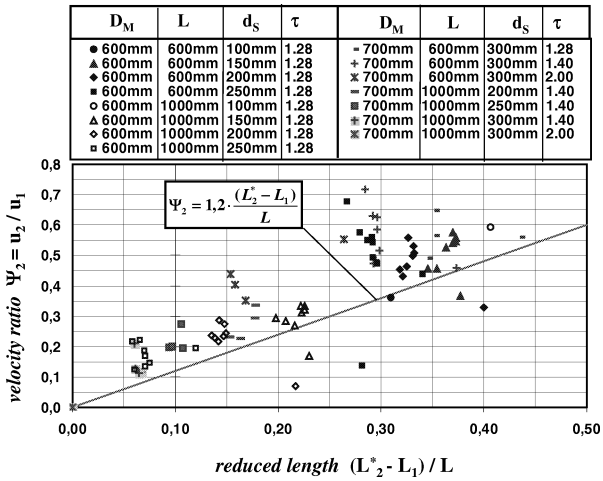

Figure 10. Velocity ratio Ψ_2 depending on the reduced difference length.

greater than L. The values of Ψ_2 show larger deviations and in some cases a dependence on b^*. In reality, the plotted values Ψ_2 are the values calculated for the most endangered tube, therefore they are the maximum values in the cross-sectional area F_{q2}. Considering the radial velocity distribution shown in *figure 6*, average values for u_2 are needed. Therefore, it makes sense to take the lower fitting line. Thereby values between $\Psi_2 = 0$ (mean flow in the whole cross-section) and $\Psi_2 = 0.6$ at a reduced difference length of 0.5 are achieved. The velocity ratio Ψ_2 can be described by a linear function:

$$\Psi_2 = 1.2\frac{L_2^* - L_1}{L} \tag{21}$$

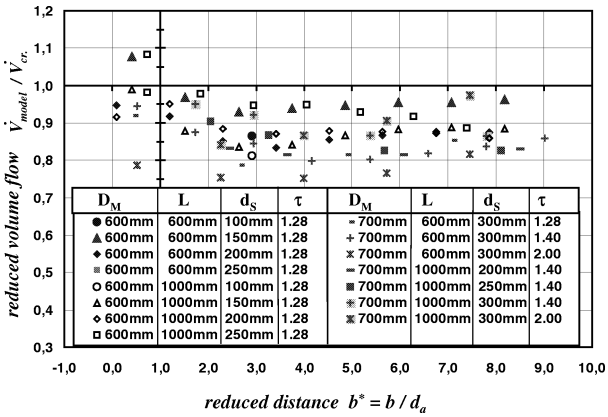

Figure 11. Model validation.

Applying the model calculation, critical volume flow rates are achieved on the safe side between 80 and 100 % of the simulated values, that corresponds to a deviation of ±10 % from an average value. In *figure 11* the volume flow rate, calculated by the derived model equations, for shell diameters $D_M = 600$ mm and $D_M = 700$ mm are shown. The results for the shell diameters $D_M = 400$ mm and 1200 mm are not shown here, but join together with the presented results.

The calculated absolute values of u_1 and $\dot{V}_{cr.}$ have been validated against measurements in single-span tubes heat exchangers [8, 11]. As for the velocity distribution, only the relative values for $\Psi_2 = u_2/u_1$ are necessary to be known. For this purpose, a validation against CFD results is adequate.

5. CONCLUSION

The presented method produces equivalent velocity distributions and corresponding cross-sectional areas in real heat exchanger bundles and enables the designer to predict the vibration excitation by fluid-elastic instability more accurate than before.

The derived equations are valid for the inlet section in the second row of normal (30°) and in the third row of rotated (60°) triangular arrays of both single- and multi-span tubes heat exchangers, considering the influence of the different energy ratios in the partial sections [1].

Up to now only cases with a central position of the inlet nozzle has been evaluated; so, the investigation is not yet concluded. The following problems have to be clarified:

- influence of the transversal flow direction in a normal triangular array (30°) at higher pitch ratios [11],
- no symmetrical mode shape function and no central position of the inlet nozzle,
- model accommodations for other tube arrangements,
- development of a model, describing the partial flow rates in the baffle windows of real heat exchangers [11].

Acknowledgement

The AIF-project No. 10608 N was promoted by the fund of the German Minister of Economics.

REFERENCES

[1] Gelbe H., Schröder K., Ziada S., Schwingungen in Wärmeübertrager-Rohrbündeln, VDI-Wärmeatlas, 8th ed., Springer-Verlag, Berlin, 1997, Chapter Oc, pp. Oc1–Oc33.

[2] Urbas L., Leyh T., Jahr M., Gelbe H., Calculation of the three-dimensional flow distribution in heat exchangers and simulation of the vibration excitation, in: ASME-PVP-Conference, Vol. 273, Flow-induced Vibration and Wear, Minneapolis, USA, 1994, pp. 234–240.

[3] Connors H.J. Jr., Fluidelastic vibration of heat exchanger tube arrays, ASME Journal of Mechanical Design 100 (1978) 347–353.

[4] Jahr M., Gelbe H., The effects of calculated velocity distribution on the vibration behaviour of tube bundles, in: ASME-PVP-Conference, Vol. 273, Flow-induced Vibration and Wear, Minneapolis, USA, 1994, pp. 7–13.

[5] Jahr M., Einflüsse von Strukturparametern und Strömungsverteilung auf das Schwingverhalten mit Luft angeströmter Rohrbündel, Dissertation D83, Technische Universität Berlin, 1995.

[6] Gelbe H., Schröder K., Bestimmung der fluidelastischen Instabilität in querangeströmten Rohrbündeln, Chemie Ing. Technik 70 (1998) 80–88.

[7] Schröder K., Gelbe H., New design recommendations for fluidelastic instability in heat exchanger tube bundles, Journal of Fluids and Structures 13 (1999) 361–379.

[8] Yeung H.C., Weaver D.C., The effect of approach flow direction on the flow induced vibrations of a triangular tube array, ASME Journal of Mechanical Design 105 (1983) 76–82.

[9] Andjelic M., Stabilitätsverhalten querangeströmter Rohrbündel mit versetzter Dreiecksteilung, Dissertation Universität Hannover, 1988 (see also: Andjelic M., Popp K., Stability effects in a normal triangular cylinder array, Journal of Fluids and Structures 3 (1989) 165–185).

[10] Austermann R., Zum Schwingungsverhalten querangeströmter Rohrbündel bei Anregung vom Galloping-Typ, Fortschritt-Berichte VDI, Reihe 11, Nr.193, VDI-Verlag, Düsseldorf, 1993 (see also: Austermann R., Popp K., Stability behaviour of a single flexible cylinder in rigid tube arrays of different geometry subjected to cross-flow, Journal of Fluids and Structures 9 (1995) 303–322).

[11] Mohr U., Schröder K., Gelbe H., The effect of approach flow direction on the fluidelastic instability of tubes in triangular tube arrays, in: 7th Int. Conference on Flow Induced Vibrations, FIV 2000, Lucerne, Switzerland, 19–21 June 2000.